Restoration of Speckled SAR Images

N. Mohan Raju*, P. Navya, N. Vyshnavi, R.Dharma Teja

Department of Electronics and Communication Engineering, Brindavan Institute of Technology and Science
Kurnool, Andhra Pradesh, India

ABSTRACT

Many coherent imaging modalities such as synthetic aperture radar suffer from a multiplicative noise, commonly referred to as speckle, which often makes the interpretation of data difficult. An effective strategy for speckle reduction is to use a dictionary that can sparsely represent the features in the speckled image. However, such approaches fail to capture important salient features such as texture. In this paper, we present a speckle reduction algorithm that handles this issue by formulating the restoration problem so that the structure and texture components can be separately estimated with different dictionaries. To solve this formulation, an iterative algorithm based on surrogate functions is proposed. Experiments indicate the proposed method performs favourably compared to state-of-the-art speckle reduction methods.

Keywords: Image Restoration, Multiplicative Noise Speckle, Synthetic Aperture Radar.

I. INTRODUCTION

Coherent imaging systems such as synthetic aperture radar (SAR), holography, ultrasound and synthetic aperture sonar suffer from a multiplicative noise known as speckle. Speckle appears when objects illuminated by coherent radiation have surface features that are rough compared with the illuminating wavelength. It is caused by the constructive and destructive interference of the coherent returns scattered by many elementary reflectors within the resolution cell. Speckle can make the detection and interpretation difficult for automated as well as human observers. In some cases, it may be important to remove speckle to improve applications such as compression, target recognition, and segmentation.

Many algorithms have been developed to suppress speckle noise. One of the simplest approaches for speckle non-coherently summing the independent images formed from L independent pieces of the phase history. The averaging process reduces the noise variance by a factor of L. However, this often results in the reduction of the spatial resolution. Other types of speckle reduction methods are based on spatial local filtering performed after the formation of the SAR image.

Various filters have been developed that avoid the loss in spatial resolution. Some of these methods are based on a window processing of the noisy image.

II. METHODS AND MATERIAL

2. Existing Methods

To overcome some of these limitations, wavelet-based methods are often utilized, in which noise shrinkage is applied to the detailed wavelet coefficients of the noisy image. Since speckle is multiplicative in nature, some of these methods often apply the logarithm transform to SAR images to convert the multiplicative noise into additive noise. After applying soft or hard thresholding to the wavelet co-efficient of the logarithmically transformed image, an exponential operation is employed to convert the logarithmically transformed image back to the original multiplicative format.

It is well known that shrinkage-based de-noising algorithms rely on the sparsity/ of the representation. A fixed transform such as a wavelet transform can represent a piecewise smooth image sparsely but it may also fail to represent an image with textures sparsely. As a result, the overall de-noising performance of a fixed

transform on an image containing both piecewise smooth and texture components can be inadequate. Several methods have been proposed that use a combined dictionary approach to image restoration. Suppose that we are given M different dictionaries D, m = 1,...,M; then one can obtain M different estimates of x by applying either hard or soft threshold to the co-efficient from each corresponding dictionary. Let ˆx be the resulting estimate from the i th dictionary. Then, a simple estimator of x is given by averaging M individual estimates. This simple method suffers from some issues in practice, as it weighs equally both good and bad quality estimates. To deal with this problem, a Bayesian framework to optimally combine the individual estimators was proposed in [27]. This method weights each estimate ˆx at each sample according to the significance that the elements in the dictionary D have in synthesizing ˆx at the same sample. This method is effective, but it can be very time consuming. A similar approach was also proposed in.

Specifically, a SAR image, considered as a function f, is to be decomposed into a sum of two components f = u+v, where u represents the cartoon or geometric (i.e., piecewise smooth) components off, and v represents the oscillatory or textured components. The second component essentially accounts for noise and the texture elements. In the proposed technique, u is estimated and is considered as the restored (de-speckled) image, while the textured components of v are not attempted to be recovered. This is problematic since discarding the texture components may result in the loss of important salient features in a SAR image. Fig. 1 provides an example of how an image separates into the structural and textured components indicating the importance of retaining these textural elements. Motivated by recent advances in sparse representation based image separation [30], we propose a similar separation based de-speckling method so that the image is decomposed into a sum of piecewise smooth and textured elements. Our formulation is based on finding sparse representations of these elements from dictionaries specifically suited to compress them, and differs significantly by not just treating the texture and noise components as complements of the cartoon-based estimated image. By taking advantage of the ability of sparse representations in our scheme to estimate, we are able to retain important salient and textured features in the final estimated image.
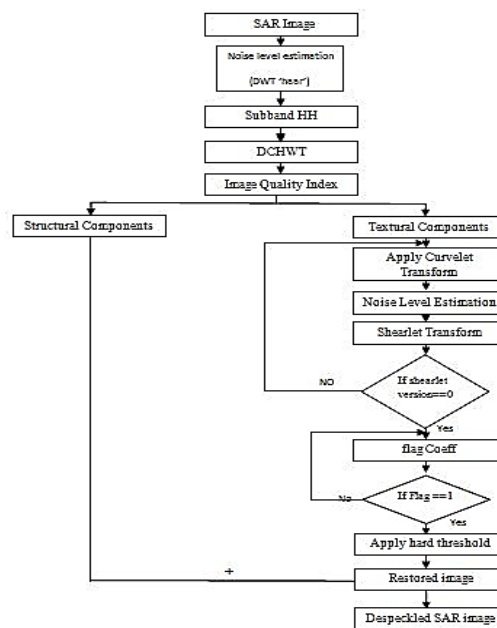
3. Proposed Method

3.1 Block Diagram

Figure 1. Block Diagram

SAR Image:

Synthetic aperture radar (**SAR**) is a form of radar which is used to create images of objects, such as landscapes − these images can be either two or three dimensional representations of the object.

DWT (Discrete Wavelet Transform):

In numerical analysis and functional analysis, a **discrete wavelet transform (DWT)** is any wavelet transform for which the wavelets are discretely sampled. As with other wavelet transforms, a key advantage it has over Fourier transforms is temporal resolution: it captures both frequency *and* location information (location in time).

Haar Wavelets:

The first DWT was invented by Hungarian mathematician Alfred Haar. For an input represented by a list of 2^n numbers, the Haar wavelet transform may be considered to pair up input values, storing the difference and passing the sum. This process is repeated recursively, pairing up the sums to provide the next scale, which leads to $2^n - 1$ differences and a final sum.

Sub band HH:

Dwt is the algorithm used to reduce dimensionality of image so it used for image compression, feature extraction process. DWT algorithm decomposes the image into 4 sub band (sub image) ie, LL, LH, HL, HH. DWT output extracts the detailed output of input image. LL is the approximate image of input image it is low frequency sub band so it is used for further decomposition process.. LH sub band extract the horizontal features of original image HL sub band gives vertical features HH sub band gives diagonal features.

DCHWT:

DCHWT stands for Discrete Cosine Haar Wavelet Transform. Each discrete cosine transform (DCT) uses N real basis vectors whose components are cosines. In the DCT-4, for example, the jth component of $\boldsymbol{v}_k$ is $\cos (j + \frac{1}{2}) (k + \frac{1}{2}) \frac{\pi}{N}$. These basis vectors are orthogonal and the transform is extremely useful in image processing. If the vector $\boldsymbol{x}$ gives the intensities along a row of pixels, its cosine series $\sum c_k \boldsymbol{v}_k$ has the coefficients $c_k=(\boldsymbol{x},\boldsymbol{v}_k)/N$. They are quickly computed from a Fast Fourier Transform.

Image Quality Index:

Image quality index, which is easy to calculate and applicable to various image processing applications. Instead of using traditional error summation methods, the proposed index is designed by modeling any image distortion as a combination of three factors: loss of correlation, luminance distortion, and contrast distortion. Although the new index is mathematically defined and no human visual system model is explicitly employed, our experiments on various image distortion types indicate that it performs significantly better than the widely used distortion metric mean squared error. Demonstrative images and an efficient MATLAB implementation of the algorithm are available.

Structural Components:

The structural components is defined as a cartoon or geometric or piecewise smooth components of an image expect the text information all information is present in structural components.

Textural Components:

Textural components represent the oscillatory or textured components. This component essentially accounts for noise and the texture elements. In order to get the salient features we are separating the structural components and textural components.

Curve Let Transform:

Curve let transform are a non-adaptive technique for multi-scale object representation. Being an extension of the wavelet concept, they are becoming popular in similar fields, namely in image processing and scientific computing.

Shear Let Transform:

In applied mathematical analysis, shear lets are a multi scale framework which allows to efficiently encode anisotropic features in multivariate problem classes. Originally, shear lets were introduced in 2006 for the analysis as well as sparse approximation of functions $f \in L^2(\mathbb{R}^2)$. They are a natural extension of wavelets to accommodate the fact that multivariate functions are typically governed by anisotropic features such as edges in images; however, wavelets as isotropic objects are not capable of capturing such phenomena.

Shear lets are constructed by parabolic scaling, shearing and translation applied to a few generating functions. At fine scales, they are essentially supported within skinny and directional ridges following the parabolic scaling law, which reads *length² ≈ width*.

Thresholding:

Thresholding is the simplest method of image segmentation. From a grayscale image, thresholding can be used to create binary images. The simplest thresholding methods replace each pixel in an image with a black pixel if the image intensity $I_{i,j}$ is less than original image some fixed constant T (that is, $I_{i,j} < T$), or a white pixel if the image intensity is greater than that constant. In the example image on the right, this results in the dark tree becoming completely black, and the white snow becoming complete white.

Image Restoration:

Image Restoration is the operation of taking a corrupt/noisy image and estimating the clean, original image. Corruption may come in many forms such as motion blur, noise and camera mis-focus.

De speckled image:

The restored image is also known as de speckled image

3.2 Image Restoration

Images are often degraded during the data acquisition process. The degradation may involve blurring, information loss due to sampling, quantization expects, and various sources of noise. The purpose of image restoration is to estimate the original image from the degraded data. Applications range from medical imaging, astronomical imaging, to forensic science, etc. Often the benefits of improving image quality to the maximum possible extent far outweigh the cost and complexity of the restoration algorithms involved.

3.2.1 Degradation Model

The most general degradation model is that of a conditional pdf for the data y given the original image x, as depicted in Fig. 1.The domains of x and y are generally (but not always) discrete. For instance, x and y could be images with the same number *N* of pixels. Figure 1: General statistical model for image restoration. We consider positive models that are representative of actual image restoration problems or at least are useful mathematical abstractions thereof.

Additive white noise

$$y = x + w$$

Linear blur plus additive white noise

$$y = Hx + w$$

where *H* represents the effects of camera or object motion, atmospheric turbulence, optics, etc. Model 3: Tomography Consider the following imaging system for transmission tomography [1, Ch. 10]. An object (typically a slice of a patient's body) is irradiated along direction *μ* by an X-ray or gamma-ray source. These high-energy photons travel through the object and are subsequently detected and counted. At each location (*x; y*) inside the object, the photon is subject to possible capture, with probability *f(x; y)dl* over an elementary path segment of length *dl*. The intensity of the surviving photons that travelled along light path *L* is therefore given by

$$\lambda(L) = \lambda_0 \exp\left\{-\int_L f(x,y)\,dl\right\}.$$

where ¸0 is the source intensity in the direction of *L*. For a light path *L* with coordinates (*s; μ*) (see Fig. 5), the normalized log-intensity at the detector is given by

$$g(s,\theta) = -\ln\frac{\lambda(L)}{\lambda_0} = \int_L f(x,y)\,dl.$$

$$g(s,\theta) = \int\int_{\mathbb{R}^2} f(x,y)\delta(-x\sin\theta + y\cos\theta)\,dx\,dy, \quad s \in \mathbb{R}, 0 \le \theta < \pi,$$

3.3 Multiplicative Noise

Image Noise is random variation of brightness or color in an image. It can be produced by any circuitry such as sensor, scanner or digital camera. Image noise is an undesirable signal, it's produce by image capturing device that add extra information. In many cases, it reduces image quality and is especially significant when the objects being imaged are small and have relatively low contrast. This random variation in image brightness is designated noise. This noise can be either image dependent or image independent.

3.3.2 Speckle Noise

Speckle noise is multiplicative noise. This type of noise occurs in various imaging systems such as Laser, Medical, Optical and SAR imagery. The source of this noise is a form of multiplicative noise in which the intensity values of the pixels in the image are multiplied by random values. Speckle noise in image is serious issue, causing difficulties for image representation. It is caused by coherent processing of backscattered signals from multiple distributed targets. The fully developed speckle noise has the characteristic of multiplicative noise. Speckle noise in image is a multiplicative noise; it is in direct proportion to the local grey level in any area.

$$P(x,y) = a(x,y) \cdot b(x,y)$$

Here a (x,y) is original signal and b (x,y) is noise introduce into signal to produce the corrupted image P (x,y). (x,y) represent the pixel location. Speckle noise follows a gamma distribution and it is give by:

$$F(g) = \frac{g^{\alpha-1}}{(\alpha-1)!a^{\alpha}} e^{\frac{-g}{a}}$$

Where, $a\_$ is variance, g is gray level and F (g) is Gamma distribution. The figure 3.1 below shows the plot of speckle noise gamma distribution.

3.3 Statistics of Speckle Noise

The pixel-to-pixel intensity variation in SAR images has a number of consequences; the most obvious one being that the use of a single pixel intensity value as a measure of distributed targets' reflectivity would be erroneous. We know that the received signal is complex; let r and i denote its real and imaginary components. For a single-look SAR image, the intensity $I=r2+i2$ of a zone of constant reflectivity is exponentially distributed. The amplitude A, which is the square root of I, follows a Rayleigh distribution. For an N-look image and independent looks, the intensity follows a Gamma distribution.

There are several ways of obtaining N-look amplitude images in the spatial domain:

Case 1. Averaging N amplitude images;

Case 2. Averaging N intensity images, then taking the square root;

Case 3. Coherently averaging complex images by means of the Weighted Filter, then taking the square root. In case 1, the probability density function is obtained by N convolutions of Rayleigh distributions, but cannot be expressed in analytic form. In the cases 2 and 3 it can be shown that the amplitude follows a K -distribution. A usual way of characterizing the speckle level in SAR image is to compute $L=E2$ (I) $/\sigma2$ (I) over an area of constant reflectivity; L is often called ENIL (Equivalent Number of Independent Looks) and gives no information on the spatial resolution of an image. We will also use the MSE between the ideal

and noisy images (in the case where the ideal image is available), which reflects both speckle reduction and preservation of structures.

3.4 Model of Speckle Noise

An inherent characteristic of ultrasound imaging is the presence of speckle noise. Speckle noise is a random and deterministic in an image. Speckle has negative impact on ultrasound imaging, Radical reduction in contrast resolution may be responsible for the poor effective resolution of ultrasound as compared to MRI. In case of medical literatures, speckle noise is also known as texture. Generalized model of the speckle is represented as,

$$g(n,m) = f(n,m) * u(n,m) + \xi(n,m)$$

Where, $g(n,m)$ is the observed image, $u(n,m)$ is the multiplicative component and ξ (n,m) is the additive component of the speckle noise. Here n and m denotes the axial and lateral indices of the image samples. In the ultrasound imaging considers only multiplicative noise and additive noise is to be ignored. Hence, above equation can be modified as; Therefore,

$$g(n,m) = f(n,m) * u(n,m) + \xi(n,m) - \xi(n,m)$$

$$g(n,m) = f(n,m) * u(n,m)$$

3.5 Image with Different Types Noise

Quality of an image is degraded by noise. Various type of noise can come into image with different strength. Some noisy images with different level of variance is shown in figure.
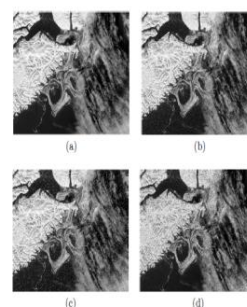
Figure 2. (a)original SAR image(b)Gaussian noisy SAR image with var 0.02(c)salt and pepper noisy SAR image with var 0.05(d) speckle noisy SAR image with var 0.08.

Exactly in phase, as in a laser, so it does not disperse over the distance between the satellite and the Earth's surface. A SAR device can measure both intensity and phase of the reflected light, resulting highly sensitive to textures. Experiments with the technique of interferometer have shown that SAR can accurately model relieves, and appears also able to reveal small changes over time. Some consequences are that it works day and night as well, it can be used to gain additional information with respect to optical imagery, especially when different polarization are available on the same platform, it needs more power than passive sensors to be operated (and can therefore only operate intermittently), and that it suffers from speckle, an artifact of interference patterns in coherent light. The SAR is radar. It uses microwave frequency radiation, which penetrates cloud and haze, so it views the Earth's land and sea surface in all weather that is the major advantage of SAR for general-purpose remote sensing. The first implementation of radar interferometer came in Earth-based observations of Venus (Rogers & Ingalls, 1969). The first reported experiments to determine terrain elevation of the Earth were by Graham (1974). Ten years later, interferometric radar experiments on the airborne system Convair-990 and on the space borne systems Seasat and SIR-B took place. Since 1990 the interest in SAR interferometer has grown due to the impressive amount of data suitable for interferometer from ERS-1 and the many airborne systems available such as the AIRSAR.

SAR images are suitable for vegetation studies, as well as ocean waves, winds, currents, seismic activity and moisture content. In practice, by properly processing the complex SAR images, it is possible to obtain high-resolution topographic maps (5 m or less height resolution), measure very small (1 cm or less) Earth surface motion over large swaths, measure water surface currents (with an accuracy around 5 cm/s) and classify land surfaces. In particular, the following main applications are worth citing:_ Ground topography: Studies on vulcanology and Earth surface motion related to differential SAR interferometer are well known. ERS-1 helps the evaluation of digital elevation models with a grid spacing of about 50 m and a height accuracy of about 5 m. AIRSAR and Do-SAR allow the evaluation of the digital elevation models with a grid spacing smaller than 10 m and a height accuracy around 1 m. The SAR-derived digital elevation models (DEM) have a big impact in the field of the topography: They are replacing the stereo DEMs derived from optical systems (Hogda, Guneriussen & Lauknes, 2002)._ Ocean surface current measurements: Ocean surface currents having speeds of less than 4 cm/s have been observed by Goldstein & Zebker (1987). _ Earth surface motion detection: Massonet (1993) shows the possibility of measuring the residual displacement caused by the earthquakes. The differential interferometer is clearly validated for long term survey of slow faults (typically 10 mm/year measured with ERS-1). This is a remarkable result, because, due to the motion errors of the aircraft, it is very difficult to implement the differential interferometer in an operational way .Land surface classification: By carrying out repeat-pass interferometer, coherence maps and change detection of SAR images can be used to provide properties of land surfaces. Results using ERS-1 data show the capability of the classification of forest, open fields, urban areas and open water (Lin, Alpers, Khoo, Lim, Lim & Kasilingam, 2001). An exemplary commercial SAR system is depicted in the Figure 2: It is a Predator Lynx synthetic aperture radar system. 3.2 Some details on imaging radar and SAR An imaging radar uses an antenna and a digital computer to store the acquired images. A radar image is generated only by the light that gets reflected back towards the antenna. Radar measures the strength and round-trip time of the microwave signals that are emitted by an antenna and reflected from a distant surface or object. Its antenna alternately transmits and receives pulses at particular microwave wavelengths (in the range of 1 cm to 1 m, which corresponds to a frequency range of about 300 MHz to 30 GHz) and polarizations (waves polarized in a single vertical or horizontal plane). About 1500 high-power pulses per second are transmitted towards the target, with each pulse having pulse duration of typically 10-50 microseconds. The pulse normally span a small band of frequencies, centered on the frequency selected for the radar; typical bandwidths are in the range 10 to 200 MHz At the Earth's surface, the energy content of the incoming radar pulse is scattered in all directions, while only a fraction of it is reflected back towards the antenna. Such energy returns to the radar as a weaker radar echo and is received by the antenna in a specific polarization (not necessarily the same as the transmitted pulse). Since the radar pulse travels at the speed of light, it is relatively straightforward to use the measured time corresponding to the roundtrip of a

particular pulse to calculate the distance or range to the reflecting object.

In the case of imaging radar, the radar moves along a light path and the area illuminated by the radar, or footprint, is moved along the surface, building the image (see Figure 3). The chosen pulse bandwidth determines the resolution in the range direction (higher bandwidth means higher resolution in this dimension), while the length of the radar antenna determines the resolution in the azimuth direction of the image (the longer the antenna, the ner the resolution in this dimension).In an imaging radar, the term "aperture" means the opening used to collect the reflected energy. Because the radar is moving with respect to the ground, the returned echoes are Doppler-shifted (negatively when the radar approaches a target, positively when it moves away). Comparing the
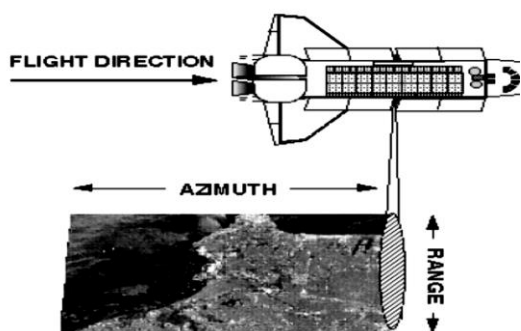
Figure 3. Exemplary representation of SAR footprint

Doppler-shifted frequencies to a reference frequency allows returned signals to be \focused" on a single point, effectively increasing the length of the antenna.

SAR data focusing consists in correctly matching the variation in Doppler frequency for each point in the image; this operation requires a precise knowledge of the relative motion between the platform and the imaged objects. Some SARs can transmit pulses in either horizontal (H) or vertical (V) polarization and receive in either H or V modes, with the resultant combinations of HH (Horizontal transmit, Horizontal receive), VV, HV, or VH. Additionally, some SARs can measure the phase of the incoming pulse and therefore measure the phase difference (in degrees) in the return of the HH and VV signals. This difference is frequently retained as an indicator of structural characteristics of the areas or objects under observation. These SARs can also measure the correlation coefficient for the HH and VV returns, which can be considered as a measure of how alike the

portions of the areas or objects are. Radar images are composed of many dots, or picture elements. Each pixel in the radar image represents the radar backscatter for an area on the ground: Bright areas represent high backscatter (bright features mean that a large fraction of the radar energy was reflected back to the radar), while darker areas in the image represent low backscatter (dark features imply that very little energy was reflected back to the antenna). Backscatter for a target area at a particular wavelength varies because of several conditions, as the size of the scatters in the target area, the moisture content of the target area, the polarization of the pulses, the values of emitted wavelengths, and the observation angles. A rule that helps interpreting the radar images is that the brighter the backscatter on the image, the rougher the surface being imaged. Flat surfaces that reflect little microwave energy always appear dark in radar images. Vegetation is usually moderately rough on the scale of most radar wavelengths and appears as gray in a radar image. Some areas not illuminated by the radar, like the back slope of mountains, are in shadow, and appear dark. Roads and freeways are at surfaces so they appear dark. Backscatter is also sensitive to the target's electrical properties, such as water content: Wetter objects appear bright and drier targets appear dark (with the exception of smooth bodies of water, which behave as at surfaces and reflect incoming pulses away, thus they appear dark). Backscatter also varies depending on the use of different polarization and observations angles: Low incidence angles (perpendicular to the surface) will result in high backscatter, while it decrease with increasing incidence angle.

III. RESULTS AND DISCUSSION

In this section, we present the results of our proposed De-speckling algorithm and compare them with the enhanced Lee filter and some recent state-of-the-art methods. We also compare our results with a Stein–Block thresholding (SBT) method proposed in. This method was shown to be nearly mini-max over a large class of images in the presence of additive bounded noise. This method requires a threshold parameter, which we set to the theoretical value 4.505 as derived in. Furthermore, we compare the performance of our combined dictionary-based approach to de-speckling with that of a fixed transform-based de-speckling

method. In particular, we apply soft thresholding on the sub-band coefficients of the wavelet transform. We call the resulting method wavelet-based thresholding (WT). For the MCA method, we use the curvelet transform to represent the piecewise smooth component and 2D-DCT to represent the texture component. In Fig., we display the test images used for different Experiments in this paper. In these experiments, we use the relative error (RE) and the equivalent number of looks (ENL)
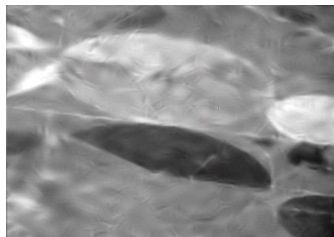

(a)

(b)

(c)

(d)

Figure 4. (a) Noisy image, $L = 4$, $RE = 0.498$. (b) Restored image using our Method, $RE = 0.118$. (c) Noisy image, $L = 4$, $RE = 0.500$. (d) Restored image using our method, $RE = 0.065$.

IV. CONCLUSION

We proposed another technique for dot lessening in SAR symbolism focused around differentiating a picture into different segments. Interesting to this methodology is the capacity to utilize particular lexicons of representations suited for detachment with an iterative plan that has the capacity hold critical gimmicks. Investigations demonstrated that this strategy performs positively contrasted with other focused routines. This new process is likewise significant for some SAR picture comprehension undertakings, for example, street location, track recognition, boat wake Identification, composition division for horticultural scenes, and coastline recognition.

Likewise, particular lexicons could be intended to be utilized with this system to catch one of a kind mark while managing with dot evacuation.

V. REFERENCES

[1] J. W. Goodman, "Some fundamental properties of speckle," *J. Opt. Soc. Amer.*, vol. 66, no. 11, pp. 1145–1150, Nov. 1976.

[2] C. Oliver and S. Quegan, *Understanding Synthetic Aperture Radar Images*. Norwood, MA, USA: Artech House, 1998.

[3] M. Amirmazlaghani and H. Amindavar, "Two novel Bayesian multiscale approaches for speckle suppression in SAR images," *IEEE Trans. Geosci. Remote Sens.*, vol. 48, no. 7, pp. 2980–2993, Jul. 2010.

[4] G. Moser and S. B. Serpico, "Generalized minimum-error thresholding for unsupervised change detection from SAR amplitude imagery," *IEEE Trans. Geosci. Remote Sens.*, vol. 44, no. 10, pp. 2972–2982, Oct. 2006.

[5] F. Argenti, T. Bianchi, A. Lapini, and L. Alparone, "Fast MAP despeckling based on Laplacian-Gaussian modeling of wavelet coefficients," *IEEE Geosci. Remote Sens. Lett.*, vol. 9, no. 1, pp. 13–17, Jan. 2012.

[6] D. Gleich and M. Datcu, "Wavelet-based despeckling of SAR images using Gauss–Markov random fields," *IEEE Trans. Geosci. Remote Sens.*, vol. 45, no. 12, pp. 4127–4143, Dec. 2007.

[7] H.-C. Li, W. Hong, Y.-R. Wu, and P.-Z. Fan, "An efficient and flexible statistical model based on generalized gamma distribution for amplitude SAR images," *IEEE Trans. Geosci. Remote Sens.*, vol. 48, no. 6, pp. 2711–2722, Jun. 2010.

[8] J.-S. Lee, "Digital image enhancement and noise filtering by use of local statistics," *IEEE Trans. Pattern Anal. Mach. Intell.*, vol. PAMI-2, no. 2, pp. 165–168, Mar. 1980.